Supporting Information

Liljeroos et al. 10.1073/pnas.1309070110

SI Materials and Methods

Electron Microscopy of Infected Cells. Electron microscopy of plastic embedded, heavy metal stained sections from infected cells was done essentially as previously reported in ref. 1, with the exception that the cell line used was HEp-2 and infection was allowed to proceed for 24 h before fixation.

Particle to Infectivity Ratio Estimation. To estimate the particle to infectivity ratio, purified virus was diluted in HBSS-Hepes buffer to a final concentration of one infectious unit per 10 μL. Then virus-containing solution was spotted on a Teflon-covered glass slide in an area of 7.06 mm^2. Virus samples were air-dried on the slide, fixed with 4% (vol/vol) formaldehyde and stained with anti–F-AF488 (green), anti-N-AF594 (red) antibody. The particles were imaged with a confocal microscope, and the number of virus particles stained with both antibodies was counted in ImageJ.

Subvolume Alignment, Classification and Averaging of the Spike Subvolumes. For analysis of the spike structures, spike densities were first selected manually in 3dmod, initial orientations estimated and the spike longitudinal axis randomized using spikeInit in PEET. For each dataset, an initial reference volume was calculated using the estimated orientations and refined with iterative alignment and averaging. Threefold averaging was applied to the long fusion protein (F) spikes as they are known to be trimers. A cylindrical mask of 7 or 20 pixels in radius was used to refine the long and short spike, respectively. Seventy-five percent of spike subvolumes were used for calculating the final averages. To assess the spike composition of the A2 and the rgRSVΔSHΔG strains, an approximately equal number of spikes [505 A2(s) (short) spikes and 442 rgRSVΔSHΔG spikes] from both were aligned and averaged together to form a composite average. The composite structure was not refined around the spike longitudinal axis and was therefore a cylindrical average of the spikes included. This average was then used as an estimate of the true subvolume for classification in PEET (2). We used six eigenvectors for the classification. Classification of the spikes between A2(l) (long) and A2(s) virions was done similarly and included 445 A2(l) and 424 A2(s) spikes. The mask used in principal component analysis in classification consisted of two superimposed cylinders with radii of 6 and 14 pixels, thus including the spike and a part of the membrane.

Subvolume Alignment and Averaging of the Matrix Protein Tube and the Ribonucleocapsid. For analysis of the matrix protein tube and the ribonucleocapsid (RNP), segments were extracted from every filament [at 11-pixel intervals for the matrix protein (M)-tube, 10 pixel intervals for the RNP]. The distances between consecutive turns of the M-tube were estimated from the tomogram, the RNP distances were taken from a previously published cryo-EM model (EMDB ID code 1622) (3). After initial alignment, 10 (RNP) or 12 (matrix helix) cylindrically symmetrical views were generated for every subvolume and they were refined limiting the rotation to prevent segments from aligning to the same orientation and position. The number of symmetrical views generated for RNP was taken from the known symmetry of the helix (3). The symmetry of the matrix helix was previously unknown, so the number of symmetrical views generated was a conservative guess taking into account the diameter of the tube and the approximate largest dimension of 7 nm of the matrix monomer (4) (PDB ID code 2VQP). The resulting model was validated by comparing the fast Fourier transforms of the tomogram and the average, and further by verifying that the final positions of the subvolumes were consistent with the helix model. Visualization of the tomograms and subvolume averages was done in 3dmod or UCSF Chimera (5). The atomic model of pre- and postfusion F (6, 7) (PDB ID codes 4GIP and 3RRT, respectively) were fitted into the subvolume spike averages in UCSF Chimera.

Estimation of Subvolume Average Resolutions. To estimate the resolution of the subvolume averages, the datasets were split into two before processing, and refined separately. The resulting half-averages were then aligned in PEET, masked with soft-edged masks and the Fourier shell correlation (FSC) curves calculated in Bsoft. The resolution value reported was at FSC 0.5.

SI Results

To measure the effect of storage on purified HRSV, we analyzed 2,000 vesicular vitrified objects larger than 100 nm in diameter from three samples stored under different conditions. The number of filamentous particles in the A2 virus micrographs decreased with storage at 37 °C for 6.5 h, followed by storage at room temperature for 18 h to 0.9%, or alternatively, by storage at −80 °C to 1.1% compared with storage at 4 °C, where 5.2% of the particles were filamentous. Freezing also resulted in more than a 90% loss of infectivity and a clear rise in particle-to-infectivity ratios (50 ± 10:1 for fresh virus and 150 ± 20:1 for frozen virus) where a virion was defined as a particle that is labeled with both anti-N and anti-F in immunofluorescence microscopy (Fig. S1). Hence, the morphology of the filamentous viruses obtained from cell culture supernatants can change because of the storage conditions, and the change in morphology correlates with a drop in infectivity.

1. Kartenbeck J, Stukenbrok H, Helenius A (1989) Endocytosis of simian virus 40 into the endoplasmic reticulum. *J Cell Biol* 109(6 Pt 1):2721–2729.
2. Heumann JM, Hoenger A, Mastronarde DN (2011) Clustering and variance maps for cryo-electron tomography using wedge-masked differences. *J Struct Biol* 175(3):288–299.
3. Tawar RG, et al. (2009) Crystal structure of a nucleocapsid-like nucleoprotein-RNA complex of respiratory syncytial virus. *Science* 326(5957):1279–1283.
4. Money VA, McPhee HK, Mosely JA, Sanderson JM, Yeo RP (2009) Surface features of a Mononegavirales matrix protein indicate sites of membrane interaction. *Proc Natl Acad Sci USA* 106(11):4441–4446.
5. Pettersen EF, et al. (2004) UCSF Chimera—A visualization system for exploratory research and analysis. *J Comput Chem* 25(13):1605–1612.
6. McLellan JS, Yang Y, Graham BS, Kwong PD (2011) Structure of respiratory syncytial virus fusion glycoprotein in the postfusion conformation reveals preservation of neutralizing epitopes. *J Virol* 85(15):7788–7796.
7. Welch BD, et al. (2012) Structure of the cleavage-activated prefusion form of the parainfluenza virus 5 fusion protein. *Proc Natl Acad Sci USA* 109(41):16672–16677.

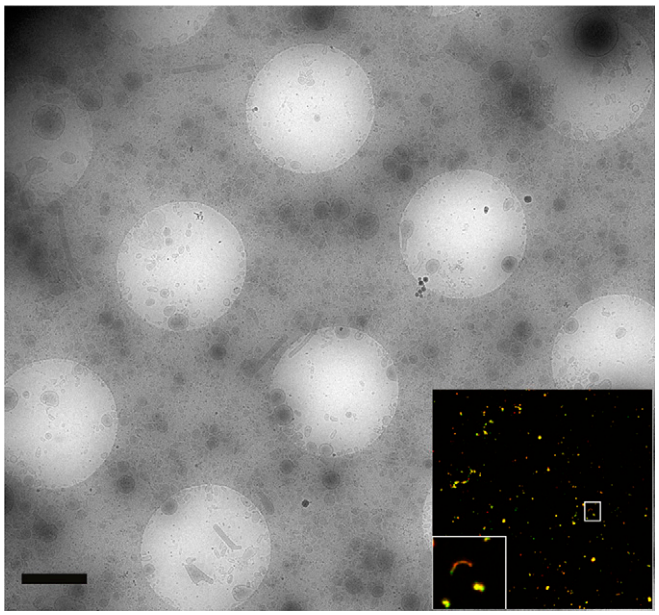

Fig. S1. The distribution of spherical and filamentous virions in an A2 sample. A low magnification micrograph of a vitrified A2 virus preparation on a holey carbon grid. (*Inset*) An immunofluorescence image of A2 virus preparation labeled with anti-F (green channel) and anti-N (red channel) is shown. Part of the image with filamentous and spherical particles labeled with both anti-N and anti-F is enlarged 10× in the white box. (Scale bar, 1 μm for the micrograph.)

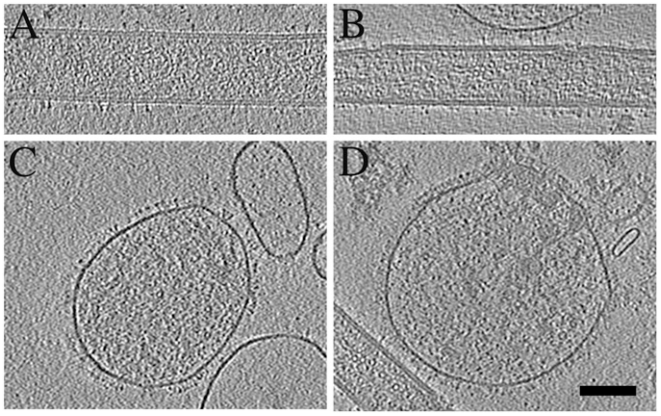

Fig. S2. Morphology of rgRSVΔG and rgRSVΔSHΔG virions. (*A*) A filamentous rgRSVΔG virion. (*B*) A filamentous rgRSVΔSHΔG virion. (*C*) A spherical rgRSVΔG virion. (*D*) A spherical rgRSVΔSHΔG virion. Images are 3.8-nm-thick slices from. (Scale bar, 100 nm.)

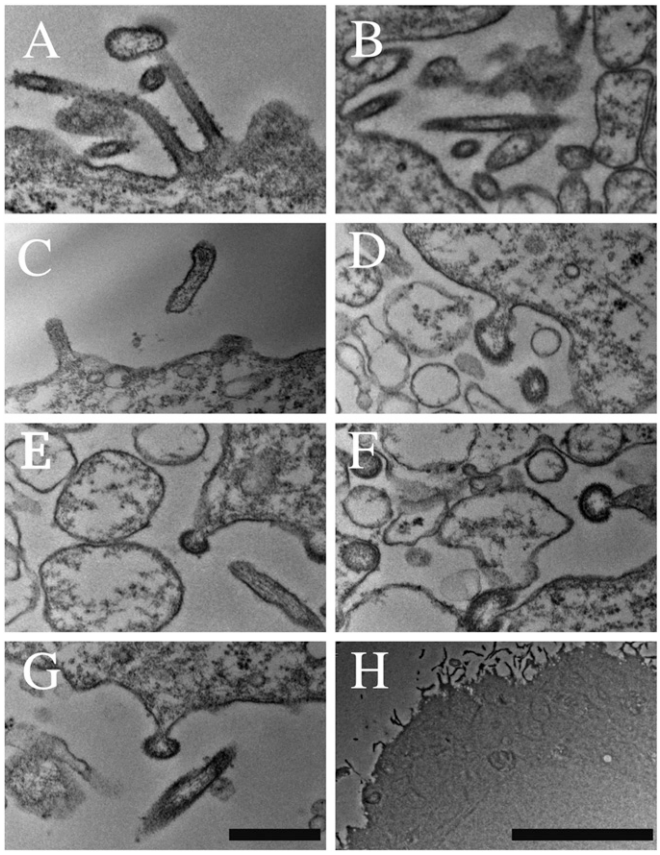

Fig. S3. HRSV budding from infected cells. (*A*–*H*) Electron microscopic images of plastic embedded, heavy metal stained sections showing filamentous protrusions on the infected cell surface. [Scale bars: 500 nm in *G*, (*A*–*G* are in the same scale); 5 μm in *H*.]

Fig. S4. An rgRSVΔG virion with a matrix layer partly detached from the membrane. A 3.8-nm-thick slice from a tomogram. (Scale bar, 100 nm.)

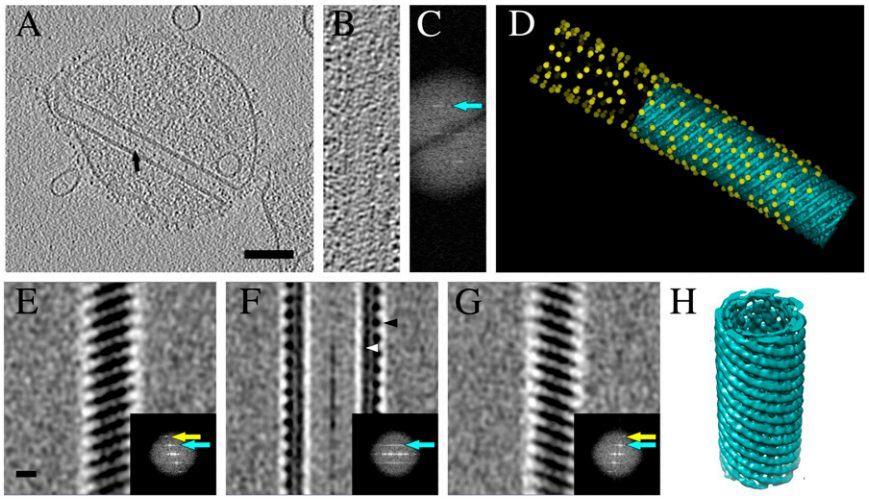

Fig. S5. Helical organization of matrix protein. (*A*) A 0.77-nm-thick slice from an rgRSVΔG tomogram showing a virion with an inside-out helical assembly of the matrix inside the particle. A spike inside the helix is indicated with a black arrow. (*B*) A tomographic slice close to the surface of the helix. (*C*) Fast Fourier transform (FFT) of the slice shown in *B*. The cyan arrow points to a layer line at 7.8-nm frequency. (*D*) A model of the M-tube showing the refined positions and orientations of the subvolumes (yellow sticks) and partial isosurface of the helix. The refined subvolume positions follow a helical pattern. (*E*–*G*) Slices (3.8 nm) from the average helix from the edges (*E* and *G*) and from the center (*F*). FFTs of the slices are shown in the *Insets*. Cyan and yellow arrows point to layer lines at 7.8-nm and 3.8-nm frequencies, respectively. Black arrowhead in *F* points to the matrix and the white arrowhead to the membrane. (*H*) Isosurface representation of the subvolume average rendered at 2 σ from the mean. (Scale bars: 100 nm in *A*, 10 nm in *E*.)

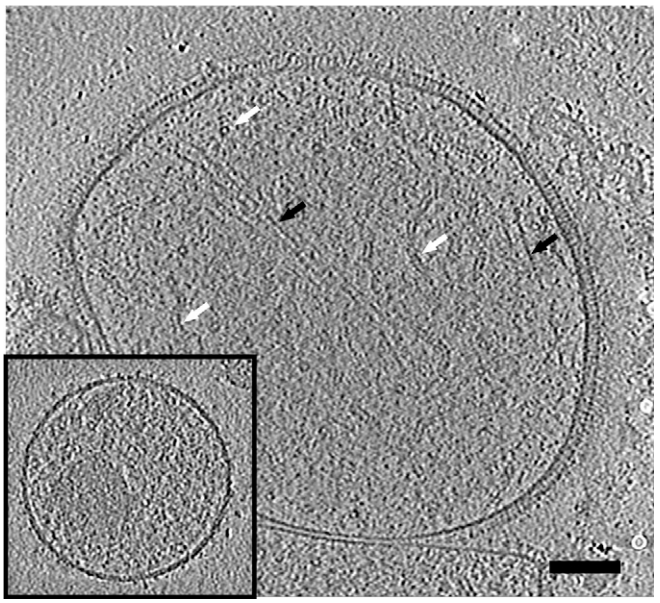

Fig. S6. The membrane of spherical virions is occupied to a varying extent by surface glycoproteins. A particle with an almost uniform layer of spikes is shown, with an inset particle containing only a few spikes (*Inset*). Filamentous actin inside the virion is marked with black arrows and RNPs with white arrows. (Scale bar, 100 nm.)

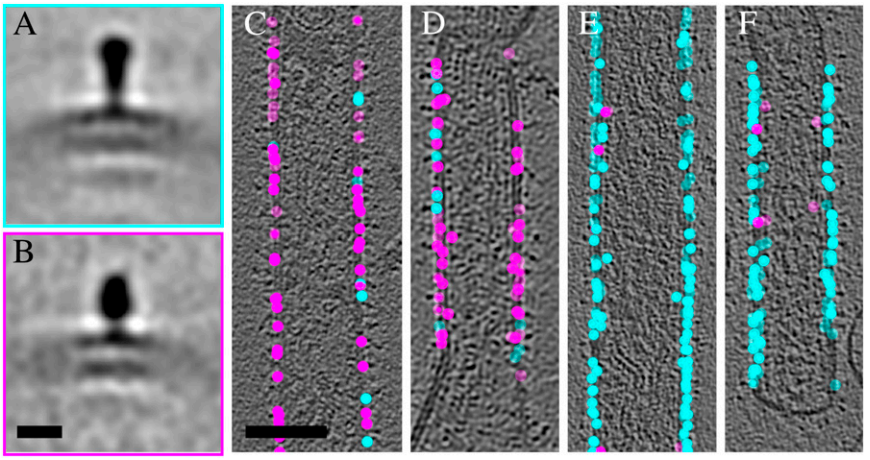

Fig. S7. F on filamentous A2 virions is found in pre- and postfusion conformations. Averages of class 1 (362 subvolumes) representing the long (*A*) and class 2 (201 subvolumes) representing the short spike (*B*) from subvolumes extracted from both A2(l) and A2(s) virions. (*C* and *D*) Positions of the classified spikes on the A2(s) and on the A2(l) virions (*E* and *F*). Cyan spheres correspond to class 1 spikes and magenta spheres to class 2 spikes. (*A*–*B*) Scale bar in (*B*) is 10 nm. (*C*–*F*) Scale bar in (*C*) is 100 nm.

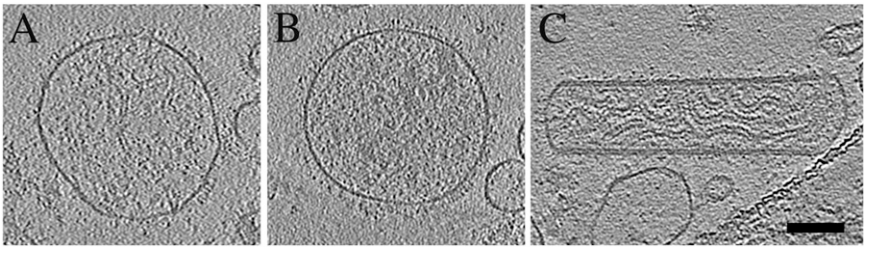

Fig. S8. The density of packing varies in spherical particles whereas filamentous particles are always densely packed. (*A*) A spherical particle with low packing density. (*B*) A spherical particle with high packing density. (*C*) A filamentous particle with approximately equal density to the spherical particle in *B*. Images are 3.8-nm-thick slices from tomograms. (Scale bar, 100 nm.)

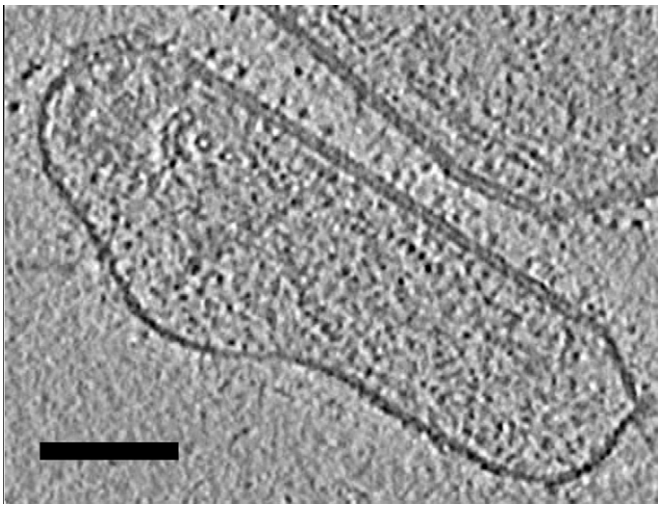

Movie S1. Tips of filaments are devoid of the matrix layer. A movie through a tomogram of a particle showing no matrix layer in the tip and an ordered assembly of the spikes on the surface. (Scale bar: 100 nm.)

Movie S1

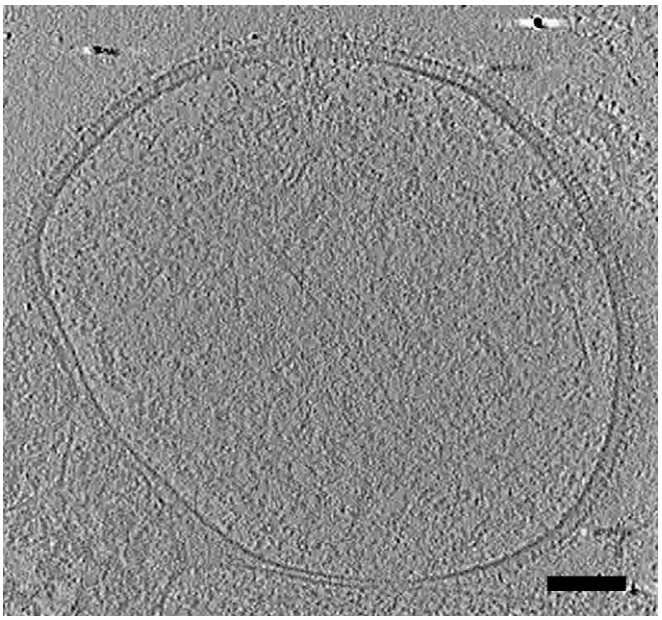

Movie S2. Some virions contain actin inside. A movie through a tomogram of large virion that contains polymerized actin inside. Fig. S6 is derived from this tomographic reconstruction. (Scale bar: 100 nm.)

Movie S2

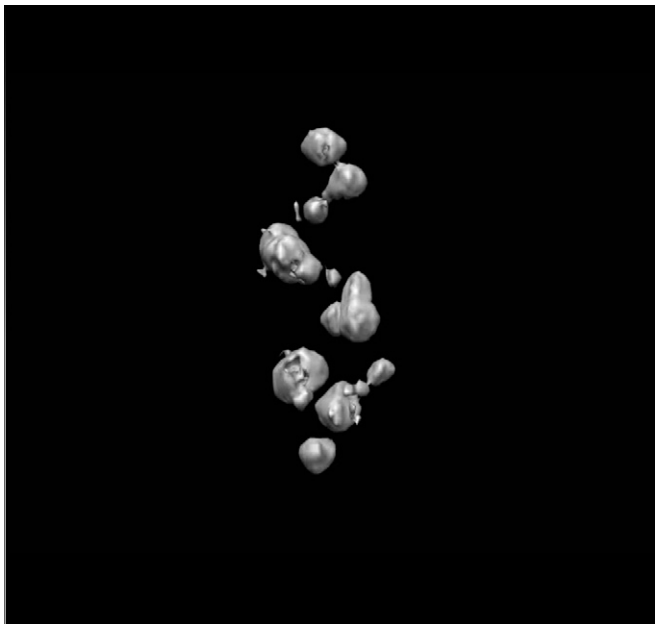

Movie S3. Negatively-stained, left-handed, silver-enhanced, DNA origami gold nanoparticle helices were used as a control for handedness. A movie showing an isosurface representation of one helix.

Movie S3